scientific reports

Check for updates

OPEN

Identification of HMGA2 inhibitors by AlphaScreen-based ultra-high-throughput screening assays

Linjia Su[1,2], Nadezda Bryan[3], Sabrina Battista[4], Juliano Freitas[1,5], Alyssa Garabedian[1,2], Federica D'Alessio[6], Miriam Romano[6], Fabiana Falanga[6], Alfredo Fusco[6], Lidia Kos[1,5], Jeremy Chambers[1,7], Francisco Fernandez-Lima[1,2], Prem P. Chapagain[1,8], Stefan Vasile[3], Layton Smith[3] & Fenfei Leng[1,2]✉

The mammalian high mobility group protein AT-hook 2 (HMGA2) is a multi-functional DNA-binding protein that plays important roles in tumorigenesis and adipogenesis. Previous results showed that HMGA2 is a potential therapeutic target of anticancer and anti-obesity drugs by inhibiting its DNA-binding activities. Here we report the development of a miniaturized, automated AlphaScreen ultra-high-throughput screening assay to identify inhibitors targeting HMGA2-DNA interactions. After screening the LOPAC1280 compound library, we identified several compounds that strongly inhibit HMGA2-DNA interactions including suramin, a century-old, negatively charged antiparasitic drug. Our results show that the inhibition is likely through suramin binding to the "AT-hook" DNA-binding motifs and therefore preventing HMGA2 from binding to the minor groove of AT-rich DNA sequences. Since HMGA1 proteins also carry multiple "AT-hook" DNA-binding motifs, suramin is expected to inhibit HMGA1-DNA interactions as well. Biochemical and biophysical studies show that charge-charge interactions and hydrogen bonding between the suramin sulfonated groups and Arg/Lys residues play critical roles in the binding of suramin to the "AT-hook" DNA-binding motifs. Furthermore, our results suggest that HMGA2 may be one of suramin's cellular targets.

The mammalian high mobility group protein AT-hook 2 (HMGA2) is a multi-functional nuclear protein highly expressed in the early embryonic stage[1]. Early studies showed that HMGA2 is related to preadipocyte proliferation & differentiation and obesity[2–4]. For example, *Hmga2* knockout mice were severely deficient in fat cells and developed pygmy phenotype[1]. The disruption of *Hmga2* gene dramatically reduced obesity of leptin-deficient mice (Lep^{ob}/Lep^{ob})[2]. These results suggest that HMGA2 is a potential target for the treatment of obesity. HMGA2 is also linked to oncogenesis. The over and/or aberrant expression leads to the formation of a variety of tumors including benign tumors, such as lipomas[5] and uterine leiomyomas[6], and malignant tumors, such as lung cancer[7,8], leukemia[9], and melanoma[10,11]. Intriguingly, HMGA2 expression level always correlates with the degree of malignancy, metastasis, and a poor prognosis[12,13], suggesting that this protein is also a therapeutic target of anti-cancer and anti-metastasis drugs[14,15]. Furthermore, HMGA2 is associated with neural and hematopoietic stem cell youth[16,17], human height[18], and human intelligence[19].

HMGA2 is a small DNA-binding protein and belongs to the HMGA family[20,21]. This protein family has four members: HMGA1a, 1b, 1c, and HMGA2[22]. HMGA1a, 1b, and 1c are different splicing products of the same gene, HMGA1 gene[23]. HMGA2 is the product of a separate gene, HMGA2 gene[24,25]. All members except HMGA1c

[1]Biomolecular Sciences Institute, Florida International University, Miami, FL 33199, USA. [2]Department of Chemistry and Biochemistry, Florida International University, 11200 SW 8th Street, Miami, FL 33199, USA. [3]Conrad Prebys Center for Chemical Genomics, Sanford Burnham Prebys Medical Discovery Institute at Lake Nona, Orlando, FL 32827, USA. [4]Istituto per l'Endocrinologia e l'Oncologia Sperimentale, CNR, Via Pansini 5, 80131 Naples, Italy. [5]Department of Biological Sciences, Florida International University, Miami, FL 33199, USA. [6]Dipartimento Di Medicina Molecolare E Biotecnologie Mediche, Università Degli Studi "Federico II" Di Napoli, Naples, Italy. [7]Department of Environmental Health Sciences, Florida International University, Miami, FL 33199, USA. [8]Department of Physics, Florida International University, Miami, FL 33199, USA. ✉email: lengf@fiu.edu

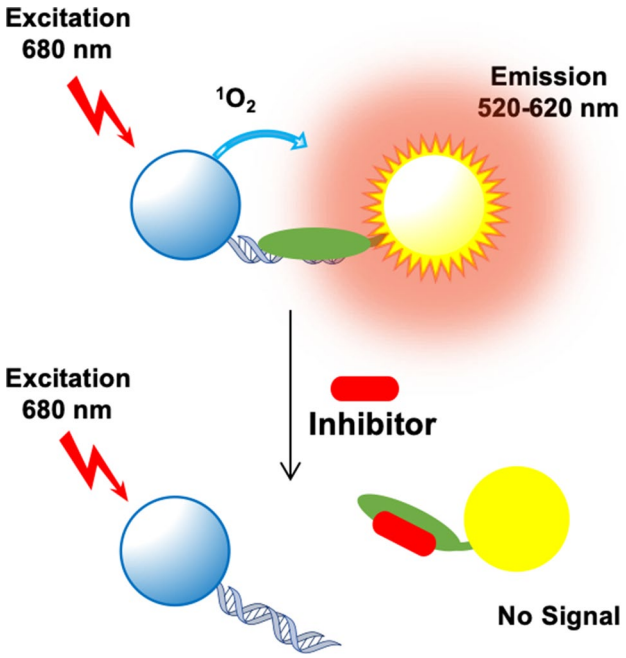

Figure 1. The AlphaScreen primary assay for HMGA2-DNA interaction. The biotin-labeled FL814 (double-stranded DNA) and the His-tagged HMGA2 (green oval) were immobilized to streptavidin-coated donor beads and nickel chelate (Ni-NTA) acceptor beads, respectively.

consist of three "AT-hook" DNA-binding motifs and a highly acidic C-terminal motif[26]. The "AT-hook" DNA-binding motifs contain a unique palindromic sequence, PGRGP, each side surrounded by one or two positively charged amino acids, i.e., Lysine or Arginine[27] and bind to the minor groove of AT-rich DNA sequences[28]. HMGA2 is an intrinsically disordered protein (IDP[29]). When it binds to AT-rich DNA sequences, the "AT-hook" DNA binding motifs adopt defined structures[30]. This disordered-to-ordered conformational transition allows HMGA2 to adapt to different AT-rich DNA sequences and to participate in different nuclear activities[20,21]. These results suggest that HMGA2-DNA interactions could be chemically intervened for therapeutic purposes[31]. Utilizing a systematic evolution of ligands by exponential enrichment (SELEX) method, we previously identified two consensus DNA sequences for HMGA2 binding: 5′-ATATTCGCGAWWATT-3′ and 5′-ATATTGCGCAWW ATT-3′, where W is A or T[26]. This result and a following study[32] suggests that HMGA2 binds and bends specific DNA sequences.

With the identification of HMGA2 as a potential target for the treatment of obesity and cancer, the next step is to search for chemical compounds that prevent HMGA2 binding to its target DNA sequences. For instance, utilizing protein–DNA interaction enzyme-linked immunosorbent assays (PDI-ELISA), we recently found several DNA-binding inhibitors including netropsin that disrupt HMGA2-DNA interactions[33]. Intriguingly, our results showed that netropsin strongly inhibited the differentiation of the mouse pre-adipocyte 3T3-L1 cells into adipocytes most likely through a mechanism by which netropsin inhibits HMGA2-DNA interactions[33]. However, DNA-binding compounds are usually too toxic to be used as anti-obesity and anticancer drugs. Novel inhibitors of HMGA2-DNA interactions that are not cytotoxic and do not directly bind DNA are required before such approaches can be considered as therapeutic applications. A high-throughput screening (HTS) strategy is needed to identify novel compounds that disrupt HMGA2-DNA binding. To achieve this, we developed an AlphaScreen-based assay of HMGA2 binding to DNA that is amenable to automated ultra HTS (uHTS) in a high-density plate format. Here we report the establishment of the assay, and the identification of several HMGA2 inhibitors including suramin, a century-old antiparasitic drug.

Results

An automated uHTS assay to identify HMGA2 inhibitors. We previously used a PDI-ELISA assay to screen a small library containing 29 DNA-binding compounds and successfully identified several small molecules that disrupt HMGA2 binding to the minor groove of AT-rich DNA sequences[33]. Although this assay performs well in a 96 well plate format, it is not suitable for automated ultrahigh throughput screening of 100,000s of compounds due to the need for streptavidin-coated assay plates and multiple wash steps. To address these limitations, we established a new assay using AlphaScreen technology. The assay entails binding a biotin-labeled DNA oligomer FL814 and His-tagged HMGA2 to streptavidin-coated donor beads and nickel chelate (Ni-NTA) acceptor beads, respectively (Fig. 1). A series of DNA binding studies were performed to determine the optimal conditions for the AlphaScreen Primary Assay (Fig. S1a–d). After these experiments, 12.5 nM of FL814 and 62.5 nM of HMGA2 were chosen for the assay. The assay tolerated up to 1% DMSO without any significant change in signal. We have previously identified two commercially available compounds netropsin and WP631

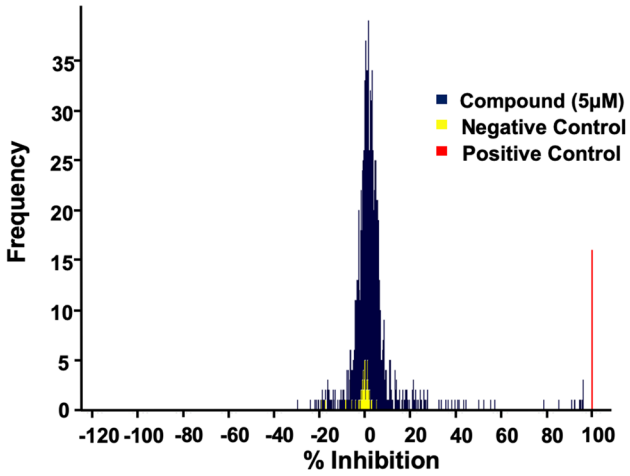

Figure 2. HMGA2-DNA pilot screens using the Sigma LOPAC1280 compound library. Netropsin was used as positive controls.

that strongly inhibit HMGA2 binding to FL814[33]. These two inhibitors are readily available for purchase and served as positive controls for HMGA2-DNA interaction inhibition in the assay. Results in Fig. S1e demonstrate that netropsin and WP631 potently inhibit HMGA2-DNA interactions with an IC_{50} of 22 and 48 nM, respectively.

In this study, we also developed a LANCE time-resolved fluorescence energy transfer (TR-FRET) assay as a secondary assay for our screening. The His-tagged HMGA2 and biotinylated oligomer FL814 were linked to Europium-labeled anti-6 × His antibody and APC-labeled streptavidin, respectively. A series of DNA binding studies were performed to determine the optimal conditions for the secondary Assay (Fig. S2). After these experiments, 12.5 nM of FL814 and 62.5 nM of HMGA2 were chosen for the assay, which is the same for the primary assay. The assay tolerated up to 0.25% DMSO without any significant change in signal (Fig. S2c). For a counterscreen assay to exclude those compounds that nonspecifically bind to the protein surface, an AlphaScreen assay of H4 peptide binding to bromodomain-containing protein 4 (BRD4) was adopted (Fig. S2e). Since we are looking for compounds with anti-metastasis or anti-obesity activities, compounds with high levels of cytotoxicity are undesirable. A cytotoxicity assay using the ATPlite Luminescence Assay System and the human epidermoid carcinoma cell line, A431, was developed to eliminate compounds that exhibit cytotoxicity. Compounds that potently and selectively inhibit HMGA2 binding to FL814, and display a $IC_{50} > 50$ μM are will be prioritized for further characterization. Those that do not will be excluded. Furthermore, potential DNA-binding compounds, i.e., DNA intercalators, minor groove binders, and DNA alkylating agents, can be identified by analyzing their chemical structures and will be excluded as well.

Screen the LOPAC1280 compound library. With the establishment of the miniaturized, automated uHTS assays, we screened the Sigma LOPAC1280 collection of pharmacologically active chemical compounds at a final concentration of 5 μM (Fig. S3a). Figure 2, Fig. S3b, and Table S1 show our results and parameters of the AlphaScreen primary uHTS assay. The following 16 compounds showed ≥ 50% inhibition of HMGA2-FL814 interactions: cisplatin, cDPCP, carboplatin, mitoxantrone, Ro 90-7501, aurintricarboxylic acid, GW5047, indirubin-3′-monoxime, 6-hydroxy-DL-DOPA, methyl-3,4-dephostatin, tyrphostin 51, (2′Z,3′E)-6-bromoindirubin-3′-oxime, reactive blue-2, JFD00244, steviol, and suramin. These 16 compounds were cherry picked and then subjected to testing in the LANCE TR-FRET secondary assay. The following seven compounds demonstrated ≥ 50% inhibition of HMGA2-DNA interactions in both uHTS assays: cisplatin, cDPCP, carboplatin, mitoxantrone, Ro 90-7501, aurintricarboxylic acid, and suramin. Dry powders of these seven compounds were purchased for additional testing in these assays. The identity of the compounds was confirmed by LC/MS, and fresh stock solutions (10 mM) were prepared in 100% DMSO. We next performed a series of titration experiments and determined the potencies (IC_{50}) values of these seven hits in the primary AlphaScreen assay, and the secondary LANCE TR-FRET assay, as well as the counter screen assay, and cytotoxicity assay. Table S2 summarizes our results. Cisplatin, cDPCP, carboplatin, and mitoxantrone are known DNA-binding agents and likely represent compounds that inhibit HMGA2-DNA interactions by binding to the AT-rich DNA sequence of FL814. Additionally, these DNA-binding compounds may also inhibit other essential cellular functions, which prevent them from further investigation. Intriguingly, although Ro 90-7501, aurintricarboxylic acid, and suramin do not bind to DNA due to their chemical properties, these three compounds strongly inhibit HMGA2-DNA interactions. Of particular interest is suramin, a highly negatively charged antiparasitic drug[34] (Fig. S4) that potently inhibits HMGA2-FL814 interactions with an IC_{50} of 2.58 μM (Fig. 3). Additionally, suramin did not inhibit H4 peptide binding to BRD4 in the counter screen assay (Fig. 3c) and is not cytotoxic to human A-431 cells (Fig. 3d, Table S2). As a final validation of suramin as a "hit" from the HTS, we confirmed its inhibitory effect on HMGA2 interactions with DNA using the PDI-ELISA assay (Table 1). Thus, suramin meets all criteria that we set for the identification of novel HMGA2-DNA inhibitors.

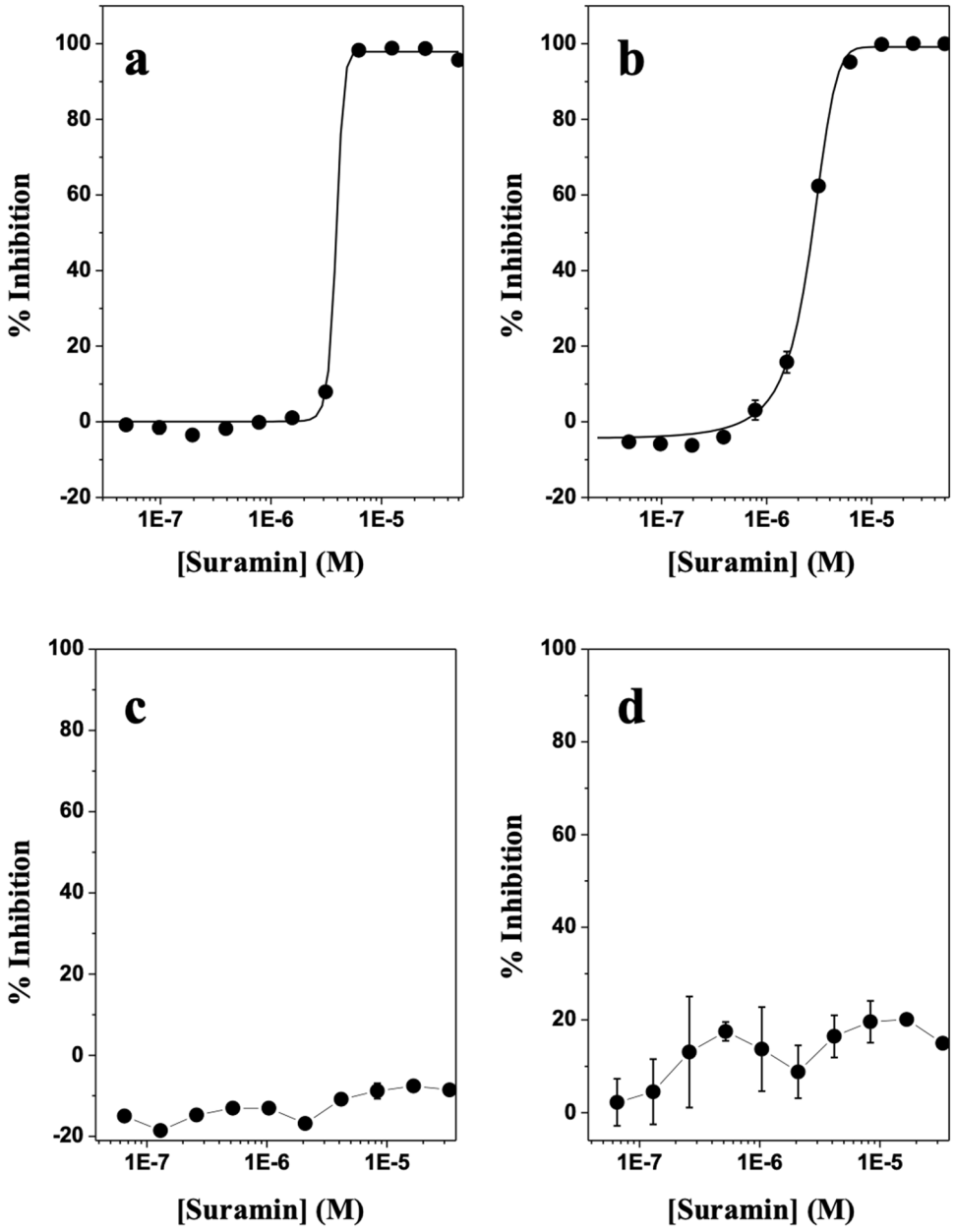

Figure 3. The discovery of suramin as a potent inhibitor of HMGA-DNA interactions. (**a**) The AlphaScreen Primay assay with IC_{50} of 2.6 μM. (**b**) The TR-FRET LANCE secondary screen. (**c**) The couterscreen assay using the BRD4 AlphaScreen Assay. (**d**) The cytotoxicity assay. All assays were described in "Methods". The standard deviation was calculated according to three independent experiments. The curve represents the best fit of a four parameter logistic that was determined by nonlinear regression. Data points represent mean ± SEM .

Suramin and analogues strongly bind to HMGA2 and ATHP3. We next sought to determine the mechanism by which suramin inhibits HMGA2-DNA interactions. Since suramin carries 6 negative charges (Fig. S4), it should not bind to DNA due to the fact that DNA is highly negatively charged. Instead, it should bind to HMGA2 because HMGA2 is positively charged[35]. ITC studies revealed that suramin physically interacts with HMGA2 (Fig. 4a, Table 1). These studies revealed that there are two types and a total of five suramin binding sites on HMGA2. The first type of three suramin binding sites has a binding constant of $4.08 \pm 0.92 \times 10^6$ M^{-1} with the following thermodynamic parameters: ΔG, −9.02 kcal/mol; ΔH −14.58 kcal/mol; and −TΔS, 5.56 kcal/mol. The second type of two suramin binding sites has a binding constant of $4.34 \pm 2.16 \times 10^4$ M^{-1} with the following thermodynamic parameters: ΔG, −6.33 kcal/mol; ΔH −6.57 kcal/mol; and −TΔS, 0.24 kcal/mol. These five suramin binding sites of HMGA2 were confirmed by our mass spectrometric experiments at high suramin to HMGA2 ratios (Fig. S5). Because HMGA2 contains three highly positively charged "AT-hook" DNA binding motifs, it is reasonable to assume that suramin strongly binds to these highly positively charged motifs through charge-charge interactions. Our ITC experiments of suramin titrating into an "AT-hook" peptide 3 (ATHP3)

Suramin and analogous	IC50 (μM)	HMGA2		ATHP3	
		K_a (M^{-1})	Binding site	K_a (M^{-1})	Binding site
Suramin	2.78 ± 0.10	$4.08 \pm 0.92 \times 10^6$	2.81	$4.06 \pm 0.32 \times 10^7$	0.98
		$4.34 \pm 2.16 \times 10^4$	2		
NF449	0.43 ± 0.18	$5.53 \pm 6.14 \times 10^7$	0.89	$1.10 \pm 7.35 \times 10^{11}$	0.86
		$8.17 \pm 1.33 \times 10^5$	1.63		
NF110	0.87 ± 0.039	$2.04 \pm 0.48 \times 10^8$	2.06	$2.17 \pm 0.17 \times 10^7$	1.01
		$7.16 \pm 0.67 \times 10^5$	1.77		
NF546	5.49 ± 2.81	$1.48 \pm 0.47 \times 10^7$	1.83	$4.28 \pm 0.47 \times 10^6$	0.81
		$3.37 \pm 8.81 \times 10^5$	1.98		
NF340	6.95 ± 9.36	$7.17 \pm 4.68 \times 10^6$	2.12	$1.89 \pm 0.16 \times 10^7$	0.8
		$2.27 \pm 0.57 \times 10^5$	0.3	$1.77 \pm 0.06 \times 10^5$	1.06
NF023	10.63 ± 0.46	$2.47 \pm 4.53 \times 10^6$	1.74	$9.75 \pm 3.47 \times 10^6$	1

Table 1. Tightly binding of suramin and analogues to HMGA2 and ATHP3.

solution confirmed this hypothesis: suramin binding to ATHPs has a binding constant of $4.06 \pm 0.32 \times 10^7$ M^{-1} and 1:1 binding molar ratio (Fig. 4b, Table 1). The following are its binding thermodynamic parameters: ΔG, − 10.38 kcal/mol; ΔH − 17.13 kcal/mol; and − TΔS, 6.75 kcal/mol.

Next, we examined the structure activity relationship (SAR) of suramin using several suramin analogues (Figs. S4, S6, S7). As shown in Table 1, all of these analogues except sodium 1-naphthalenesulfonate potently inhibit HMGA2-DNA interactions with IC50 values ranging from 0.43 to 10.63 μM (the results of sodium 1-naphthalenesulfonate are not included in Table 1). Likewise, all these chemical compounds except sodium 1-naphthalenesulfonate strongly bind to both HMGA2 and ATHP3. Intriguingly, although the negative charge is important, it is not the only parameter that determines their inhibition potency. For example, NF110 only carries 4 negative charges. However, it strongly inhibits HMGA2-DNA interactions with an IC50 of 0.87 ± 0.04 μM. In contrast, although NF023 has 6 negative charges, its inhibition IC50 was determined to be 10.63 ± 0.46 μM, tenfold higher than that of NF110. These results suggest that both the charge and structure are very important for the inhibition of HMGA2-DNA interactions by these related compounds.

Effects of suramin on tumor cells. Previous studies showed that HMGA2 plays a critical role in the epithelial-mesenchymal transition (EMT) induced by transforming growth factor-β (TGF-β)[36]. Further studies showed that HMGA2 directly binds to the promoter region of the transcriptional factor SNAIL and co-regulates SNAIL expression with intracellular transducers, Smads during the EMT induction[37]. Since HMGA proteins including HMGA2 are highly expressed in glioblastomas and glioblastoma-derived brain tumor stem cells (BTSCs)[38], where they play pivotal roles in regulating self-renewal, differentiation and symmetric/asymmetric division[38,39], BTSCs are a good cell assay system to evaluate the effect of suramin on the expression of SNAIL and several differentiation and stemness markers, such as MSI1 (Musashi RNA Binding Protein 1), ID2 (inhibitor of DNA binding 2), and OLIG2 (oligodendrocyte transcription factor)[38]. Here, we exposed two BTSC lines (BTSC#83 and BTSC#30p) to different concentrations of suramin. Consistent with the cytotoxicity studies (Table S2), up to 200 μM of suramin did not significantly affect the cell growth of these two cell lines (Fig. S8a). Intriguingly, in the presence of 100 μM and 200 μM (Fig. 5a) of suramin, cells were stimulated to adhere to the bottom of the well and extend neurite-like structures (as in BTSC#83; Fig. 5a, top panel) or acquire flat epithelial morphology (as in BTSC#30p; Fig. 5a, bottom panel), suggesting induction of differentiation in both BTSC cell lines. Western blotting and qRT-PCR experiments showed that suramin slightly reduced the expression of HMGA2 and HMGA1 in both cell lines (Fig. 5b,c; data not shown). Nevertheless, suramin significantly reduced the expressions of SNAIL, MSI1, and ID2 (Fig. 5c, Fig. S8b,d,e) and, in contrast, increased the expression of OLIG2, an oligodendrocyte differentiation marker[38] (Fig. 5c). Our previous results showed that silencing of another AT-hook protein HMGA1 in BTSC#83 and BTSC#30p downregulated MSI1 expression and induced cells to adhere and extend neurite-like structures or acquire flat epithelial morphology[38]. Fig. S8 also shows that silencing of HMGA1 induces reduction in ID2 expression in BTSC#30p but not in BTSC#83 (Fig. S8c). Similarly, treatment with 100 μM Suramin for 48 h induces reduction in ID2 expression in BTSC#30p but not in BTSC#83 (Fig. S8d,e), suggesting that HMGA silencing produces similar effects to suramin treatment. Although these results support a hypothesis by which suramin targets HMGA-DNA interactions in these two BTSC cell lines and therefore induces their differentiation, suramin may also work with other cellular components/enzymes, such as protein-tyrosine phosphatases[40] and various growth factors[41], to achieve its biological functions.

Next, we examined whether suramin is able to dissociate HMGA2 from its target DNA sequences inside cells. Since the ID2 gene promoter region contains multiple AT-rich DNA sequences and can be regulated by HMGA2[36,37] presumably through binding to these AT-rich DNA sequences, Chromatin Immunoprecipitation Analysis (ChIP) was performed to determine whether suramin could dissociate HMGA2 from the ID2 gene promoter region. The role of HMGA1 and HMGA2 in regulating ID2 transcription was confirmed by analyzing its expression in mouse embryonic fibroblasts (MEFs) knock-out for HMGA1, HMGA2, and the A1/A2 double mutant, respectively[42]. These three knock-out MEFs showed a significant down-regulation of ID2 expression (Fig. S9), indicating that both HMGA1 and HMGA2 can regulate the ID2 expression. We identified two

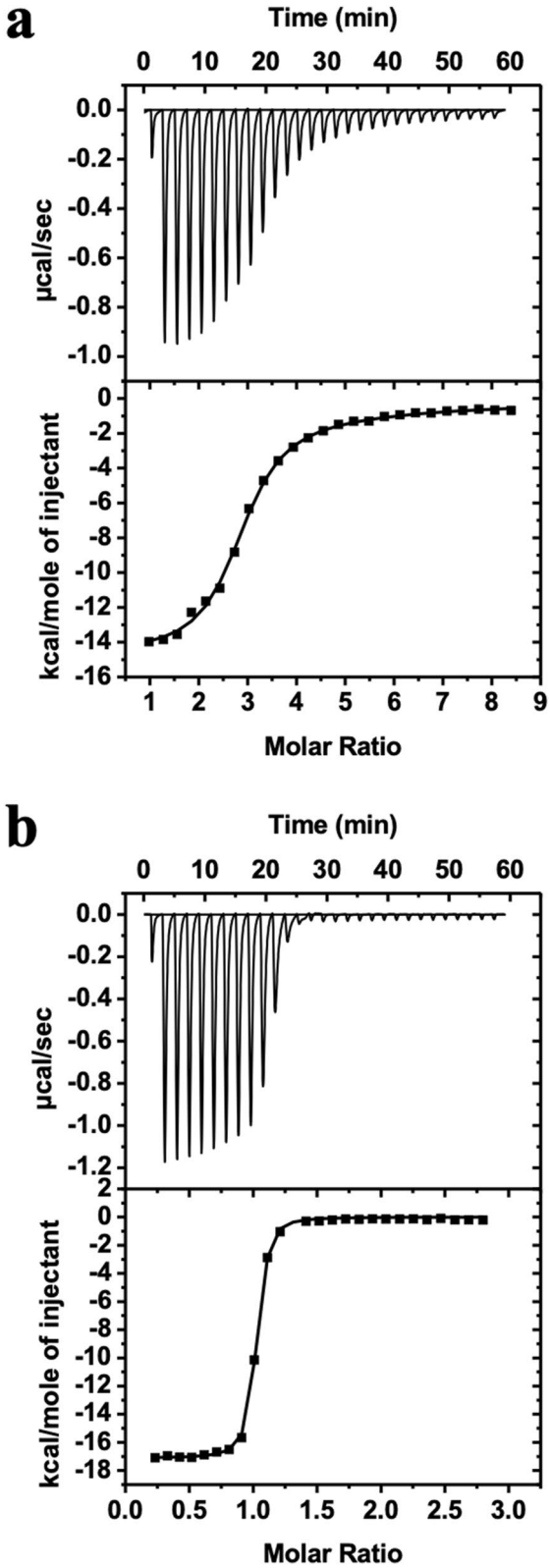

Figure 4. Sample raw data from isothermal titration calorimetry (ITC) experiments for the titration of suramin to HMGA2 (**a**) and ATHP3 (**b**). ITC experiments were performed according to conditions as described in "Methods". The ITC data were fit using the software supplied by the manufacturer to yield thermodynamic parameters.

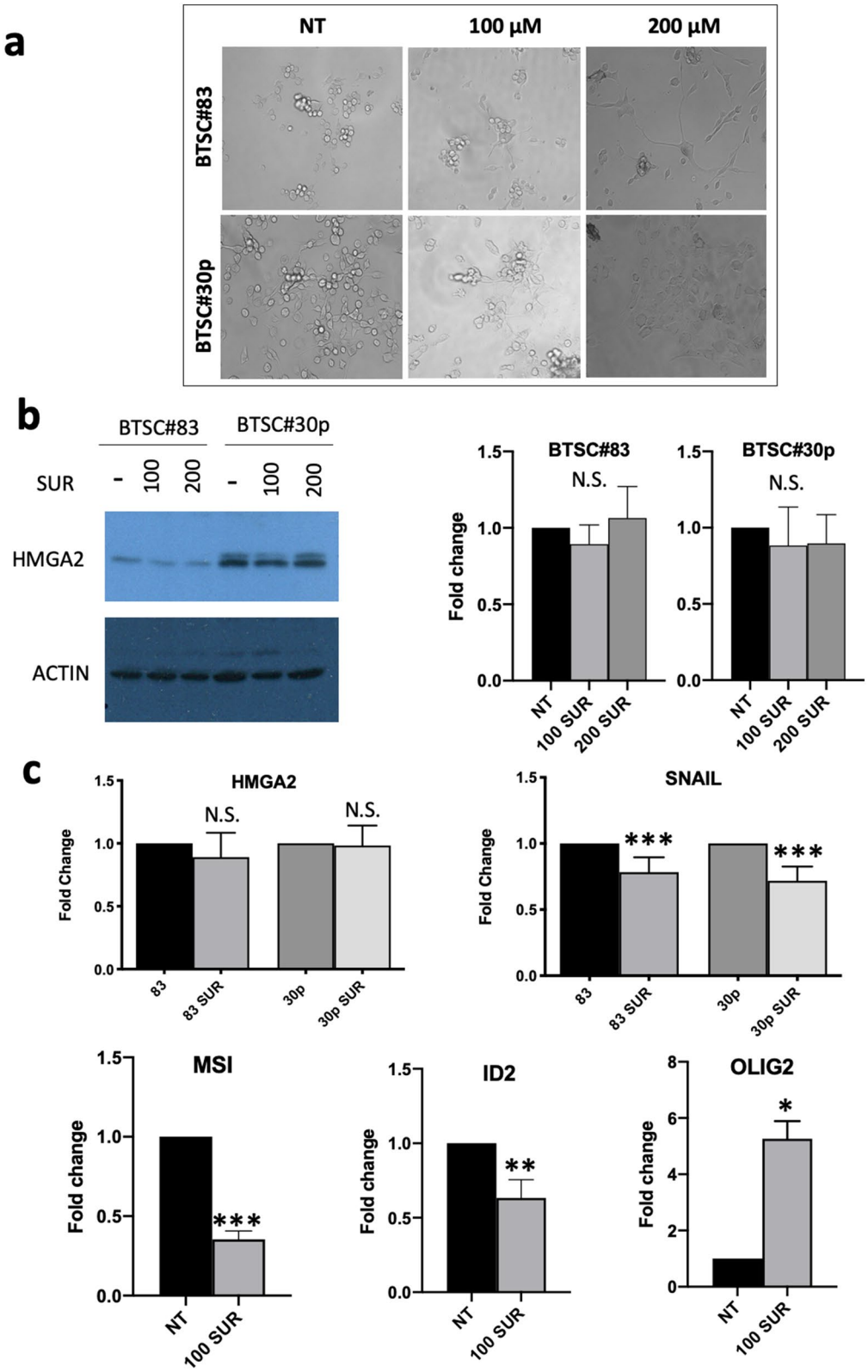

Figure 5. Suramin induces the differentiation of brain tumor stem cells (BTSCs) #83 and #30p. (**a**) Light Microscopy of BTSC#83 and BTSC#30p treated with various concentrations of suramin for 6 days, compared to non-treated (NT) cells. (**b**) Western blot analysis (left panel) and densitometry (right panels) of HMGA2 expression after the 6-day treatment of suramin. This image was generated using two different blots of the same Western blot by antibodies against HMGA2 (the top panel) and actin (the bottom panel), respectively. The original images are provided in the supplemental information Fig. S11. (**c**) Expression of HMGA2, SNAIL, MSI1, ID2, and OLIG2 in suramin-treated BTSCs. qRT-PCR analyses of HMGA2 and SNAIL in BTSC#83 and BTSC#30p treated with suramin 100 µM for 48 h, compared to non-treated cells. qRT-PCR analyses for stemness (MSI1 and ID2) and differentiation markers (OLIG2) in BTSC#30p, treated with suramin 100 µM for 9 days. Fold changes are normalized for actin expression. Data represent the mean value +/− SD of two or three independent experiments performed in duplicate. (*$p \leq 0.05$; **$p \leq 0.01$; ***$p \leq 0.001$; Student's t test).

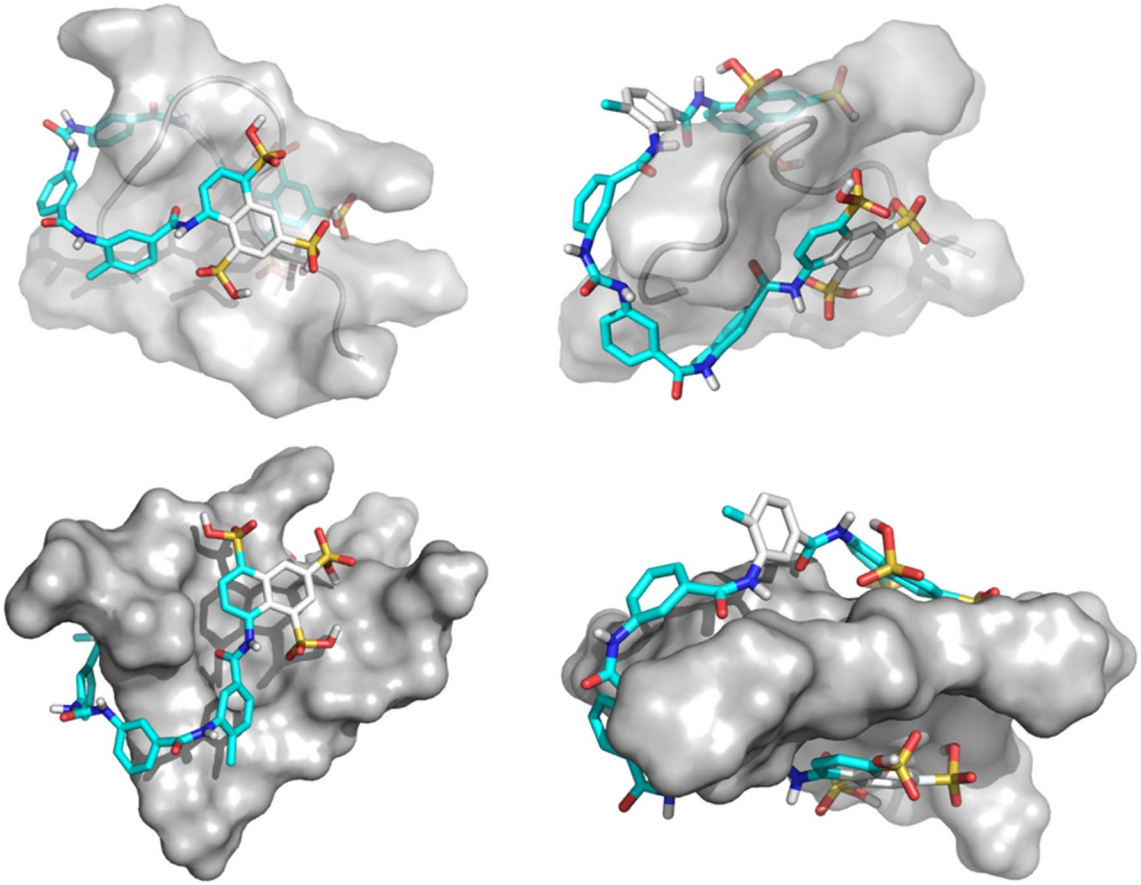

Figure 6. The simulated structure of the suramin-ATHP3 complex obtained by molecular docking and simulations.

AT-rich regions, hereafter indicated as "region A" and "region B", in the human ID2 promoter, containing the HMGA2 consensus sequence[26] (Table S2) for our ChIP experiments. Due to availability, the high proliferation rate, and the expression of HMGA proteins, the anaplastic thyroid carcinoma cell line 8505c was used. Briefly, after 8505c cells were treated with 100 and 200 μM suramin for 6 days, the ChIP experiments were performed. Fig. S10 shows our results. In the absence of suramin, the sample immunoprecipitated with the anti-HMGA2 antibody is enriched both in region A and B (Fig. S10a), indicating that HMGA2 is able to bind to both regions. Unexpectedly, we did not detect significant HMGA2 binding reduction in the presence of 100 μM of suramin (Fig. S10). Nevertheless, 200 μM of suramin caused a drastic reduction in the enrichment of the anti-HMGA2 precipitated sample with respect to the sample immunoprecipitated with IgG only, indicating the loss of the binding of HMGA2 to regions A and B. These results demonstrate that suramin can inhibit HMGA2-DNA binding in 8505c cells. Similarly, the mRNA expression level of ID2 was significantly decreased in the presence of 200 and 400 μM of suramin (Fig. S10b).

Discussion

In this article, we report the development of a miniaturized, automated AlphaScreen uHTS assay to identify small molecule inhibitors targeting HMGA2-DNA interactions. This uHTS assay has excellent screening parameters with a Z′ and S/B ratio at 0.83 and 438, respectively (Table S1). After screening the LOPAC1280 compound library, we found that suramin, a highly negatively charge anti-parasitic drug that is used to treat African sleeping sickness and river blindness[43,44], is a potent inhibitor of HMGA2-DNA interactions. Further, our results show that suramin's inhibition of HMGA2-DNA interactions stems from its binding to HMGA2 with high affinity, particularly to ATHPs. Our molecular modeling studies confirmed this hypothesis (Fig. 6). The suramin-ATHP3 complex shows that the suramin sulfonated groups are close to the Arg and Lys residues, providing ionic/hydrogen-bond interactions. The ring structures at the two ends of suramin are folded to embrace the central proline ring from either side of the residue.

DNA-binding proteins, such as transcriptional factors are excellent targets for anticancer therapy[45]. Indeed, several clinically important anticancer drugs, such as doxorubicin and cisplatin[46,47], bind to DNA, disrupt protein-DNA interactions, and as a result prevent DNA-binding proteins including transcriptional factors from binding to their target DNA sites[48]. However, a major disadvantage of these anticancer drugs is that they bind to DNA nonspecifically. Consequently, they kill cancer cells as well as normal cells causing serious side effects. Therapeutically active compounds that specifically block oncogenic transcriptional factors from binding to their DNA recognition sites would be superior medicines. Such medicines would be expected to have fewer, less severe

side effects, thereby potentially increasing the dose and duration of chemotherapy and perhaps improving treatment outcomes as well as quality of life. Transcription factors are widely considered to be "undruggable" because they usually do not have enzymatic activities, and lack deep pockets to accommodate drug-like molecules[49]. Further, the lack of HTS assays to identify inhibitors from small molecule repositories also contributes to the perceived undruggable nature of transcriptional factors[33]. Our results refute these notions, at least with respect to the potential druggability of HMGA2. Previously, we developed protein–DNA or protein–RNA interaction enzyme-linked immunosorbent assays (PDI-ELISA or PRI-ELISA) to identify inhibitors targeting specific protein-nucleic acids interactions[33]. These methods are versatile and can be applied to any nucleic acid binding proteins as long as an antibody is available. In fact, one may use tagged proteins, such as His-tagged proteins so that antibodies against His-tag can be used in PDI-ELISA or PRI-ELISA. Regardless, as we pointed out above, because streptavidin-coated 1536-well plates are expensive, PDI-ELISA or PRI-ELISA cannot be configured into a miniaturized, automated uHTS assay in a 1536 well plate format. Additionally, too many washing steps were used, which make PDI-ELISA or PRI-ELISA a "lengthy" procedure and unsuitable for automated uHTS studies. Here we showed that AlphaScreen assays could be utilized to screen for inhibitors against HMGA-DNA interactions by using His-tagged HMGA2 linked to nickel chelate (Ni-NTA) acceptor beads. The use of AlphaScreen uHTS assays has several advantages. Because His-tag can be added to most of DNA-binding proteins and usually does not interfere with their DNA binding activities, AlphaScreen assays can be used to screen and identify inhibitors targeting most DNA-binding proteins. Another advantage is that AlphaScreen uHTS assays are cost-effective. For instance, in this study, only one 1536-well plate was used in the screening of the LOPAC1280 compound library. It is anticipated that AlphaScreen uHTS assays using His-tagged DNA binding proteins will be utilized to identify inhibitors for other DNA-binding proteins in the future.

The most intriguing result of this uHTS study is the identification of suramin as a potent inhibitor for HMGA2-DNA interactions. The inhibition is likely through a mechanism by which suramin tightly binds to highly positively charged ATHPs. This is not surprising because suramin, a polysulphonated naphylurea, carries 6 negative charges at physiological conditions (Fig. S4). As shown in Fig. 6, charge-charge interactions and hydrogen bonding between the suramin sulfonated groups and Arg/Lys residues play critical roles in the binding of suramin to ATHPs. This inhibition mechanism is different from that of netropsin and other DNA minor groove binders that prevent HMGA2 from binding to the minor groove of AT-rich DNA sequences[15,33]. In fact, suramin is the first chemical compound that was found to tightly bind to the intrinsically disordered protein (IDP) HMGA2 and the "unstructured" DNA-binding motif ATHPs. Since HMGA1 proteins also carry multiple "AT-hook" DNA-binding motifs[50,51], suramin is expected to strongly inhibit HMGA1-DNA interactions as well. Furthermore, it is reasonable to predict that suramin tightly binds to many positively charged motifs on protein surface that contain lysine and/or arginine residues.

Suramin is a century-old drug synthesized in the 1920s by Bayer to treat human African trypanosomiasis (HAT)[52]. However, the mechanism or mode of action is still unknown[53]. Suramin is usually administered by intravenous injection due to the poor intestinal absorption[34] and binds to serum proteins, such as albumin and low-density lipoprotein (LDL), immediately after administration[34]. It is believed that the parasite takes up the drug through receptor-mediated endocytosis of the protein-bound drug[54]. Suramin is highly effective against blood-stream forms of the parasite but not very active against procyclic trypanosomes[55]. Since the bloodstream forms of *Trypanosoma brucei* lacks a functional mitochondrion and entirely depend on glycolysis for their energy needs, this led to the hypothesis that the glycolytic pathway of the parasite is the target of the drug[56]. However, so far there is no direct evidence to support this hypothesis[34]. Another interesting feature of *T. brucei* is that its mitochondrion contains the so-called kinetoplast DNA (kDNA), comprising of ~ 73% AT base pairs[57]. Recent studies showed that certain DNA minor groove-binding compounds were able to enter the mitochondrion of *T. brucei*, bind to AT sequences of kDNA and, as a result, cause cell death[58]. It was suggested that these minor groove-binding compounds might disrupt the functions of kDNA binding proteins, such as the TbKAP6 protein that is essential for kDNA replication and maintenance and also for cell viability[59]. TbKAP6 contains two HMG boxes and binds to DNA minor groove[59]. Interestingly, this protein carries several highly positively charged motifs similar to ATHP[59]. One possibility is that suramin tightly binds to these positively charged motifs in TbKAP6 and prevents its binding to kDNA. Further studies are needed to support this hypothetic mechanism.

Another interesting function of suramin is its well-studied anticancer and anti-metastasis activities[41,60,61] although the mechanism is still obscure. Possible mechanisms include inhibiting important enzymes, such as cullin-RING E3 ubiquitin ligases[62], protein-tyrosine phosphatases[40], and blocking various growth factors binding to their receptors[41]. In fact, suramin has "so many" targets that its cellular and physiological activities are expected to stem from not just one single target but multiple targets[63]. Here we reveal another potential target, HMGA2 and/or HMGA proteins for this intriguing small molecule. It is possible that binding of suramin to HMGA2 prevents the protein from binding to the target DNA sequence of the SNAIL promoter[37] and decreases the expression of SNAIL (Fig. 5c)[36,37]. The differentiation of BTSCs induced by suramin is consistent with this hypothesis (Fig. 5a). Our ChIP analysis showing that high concentrations of suramin can dissociate HMGA2 from its target DNA sequences inside cells is also consistent with this hypothesis (Fig. S10). Nevertheless, it will be difficult to design experiments demonstrating that HMGA2 and/or HMGA proteins are the suramin's only target or main target in cells. What we learned so far is that suramin likely prefers binding to positively charge motifs on protein surface similar to the way it binds to the "AT-hook" DNA-binding motifs (Fig. 6). It is also possible to identify a specific inhibitor for HMGA2 and HMGA proteins with the established uHTS in the future. Please note that suramin has several disadvantages for further development. First, suramin binds to many proteins in vitro and in vivo. It may not be very specific for HMGA2 targeting. Secondly, suramin is not orally bioavailable and must be given intravenously. Third, it has limited bioavailability through tissue due to the fact that 98% of the drug are protein bound in blood serum. Furthermore, suramin causes a fair number of side effects and unpredictable pharmacokinetics.

Methods

Materials. The His-tagged mammalian HMGA2 was purified using a Ni-NTA agarose column followed by an SP Sepharose fast flow column as described previously[26]. An extinction coefficient of 5810 M^{-1} cm^{-1} at 280 nm was used to determine its concentration[26]. Biotin-labeled DNA oligomer FL814 carrying a specific SELEX binding site of HMGA2[26,33] was purchased from Eurofins MWG Operon, Inc. AlphaScreen histidine (nickel chelate) detection kits containing nickel chelate acceptor beads and streptavidin donor beads (#6760619M), LANCE Ultra ULight-anti-6xHIS (#TRF0105) and LANCE Eu-W1024 Streptavidin (#AD0062), as well as 1536 well Optiplates plates (#6004290) were purchased from Perkin Elmer. Netropsin was purchased from Sigma and used without further purification. Suramin and NF023 were purchased from MilliporeSigma, Inc. Sodium 1-Naphthalenesulfonate was obtained from TCI America, Inc. NF110, NF340, NF449, and NF546 were purchased from Tocris Biosciences. His-tagged BRD4-BD1 was purchased from BPS Bioscience (#31042). Pre-acetylated Biotin-Histone 4 Peptide was purchased from AnaSpec (#64989-025). Bovine serum albumin fraction V (#A7888), CHAPS (#C3023-25G), and LOPAC1280 library (#LO1280) were purchased from Sigma Aldrich. Human epidermoid carcinoma A-431 cell line was purchased from the ATCC (ATCC-CRL-1555). DMEM media was purchased from Thermo Fisher (Gibco #11995), 100 × Penicillin/Streptomycin solution (#30-002-CI), DPBS (#21-031-CV), 0.25% Trypsin in HBSS (#25-050-CI), 200 mM L-glutamine (#25-005-CI), white high base 1536 well plates (#4570), and sterile white high base 1536 well plates (#4571) were purchased from Corning. The control compound MG-132 was purchased from Promega (#G932B). ATP-Lite 1-step was purchased from Perkin Elmer (#6016739).

HMGA2 AlphaScreen ultra HTS assay. Using a Labcyte Echo 555 acoustic dispenser 5 nL of DMSO were added to columns 1–4 and 45–48 of a white 1536 well plate, while 5 nL of 2 mM compounds in DMSO were added to columns 5–44. Using a Beckman BioRAPTR FRD bulk reagent dispenser 1 µL of assay buffer (30 mM Citrate, 300 mM NaCl, and 0.005% Tween 20) was added to columns 1 and 2. Next 1 µL of assay buffer containing 125 nM HMGA2 was added to columns 3–48 with a Beckman BioRAPTR FRD bulk reagent dispenser. Finally, 1 µL of assay buffer containing 25 nM FL814 was added to every well of the plate using a Beckman BioRAPTR FRD bulk reagent dispenser. The plate was then centrifuged at 200 × *g* for 1 min. After 30 min at room temperature, 2 µL of bead buffer (10 mM HEPES, 300 mM NaCl and 0.005% Tween 20) containing 20 µg/mL anti-6xHIS acceptor beads and 20 µg/mL streptavidin donor beads were dispensed into every well using a Beckman BioRAPTR FRD bulk reagent dispenser. The plates were then centrifuged at 200 × *g* for 1 min. After 1 h at room temperature the plates were read on a Perkin Elmer Envision multimode plate reader in AlphaScreen mode.

HMGA2 Lance assay. Using a Labcyte Echo 555 acoustic dispenser 5 nL of DMSO were added to columns 1–4 and 45–48 of a white 1536 well plate, while 5 nL of 2 mM compounds in DMSO were added to columns 5–44. Using a Beckman BioRAPTR FRD bulk reagent dispenser 1 µL of assay buffer (10 mM Tris, 300 mM NaCl and 0.005% Tween 20) was added to columns 1 and 2. Next, 1 µL of assay buffer containing 125 nM HMGA2 was added to columns 3–48 with a Beckman BioRAPTR FRD bulk reagent dispenser. Finally, 1 µL of assay buffer containing 25 nM FL814 was added to every well of the plate using a Beckman BioRAPTR FRD bulk reagent dispenser. The plate was then centrifuged at 200 × *g* for 1 min. After 30 min at room temperature 1 µL of assay buffer containing 250 nM LANCE Ultra ULight-anti-6xHIS and 1 µL of assay buffer containing 12 nM LANCE Eu-W1024 Streptavidin was dispensed into every well using a Beckman BioRAPTR FRD bulk reagent dispenser. The plates were then centrifuged at 200 × *g* for 1 min. After 1 h at room temperature the plates were read on a Perkin Elmer Envision multimode plate reader in TR-FRET mode (excitation @340 nm, first emission at @665 nm, second emission at 615 nm).

BRD4 AlphaScreen assay. Using a Labcyte Echo 555 acoustic dispenser 5 nL of DMSO were added to columns 1–4 and 45–48 of a white 1536 well plate, while 5 nL of 2 mM compounds in DMSO were added to columns 5–44. Using a Beckman BioRAPTR FRD bulk reagent dispenser 1 µL of assay buffer (50 mM HEPES, 100 mM NaCl, 0.1% BSA and 0.0005% CHAPS) was added to columns 1 and 2. Next, 1 µL of assay buffer containing 50 nM BRD4 was added to columns 3–48 with a Beckman BioRAPTR FRD bulk reagent dispenser. Finally, µL of assay buffer containing 50 nM peptide was added to every well of the plate using a Beckman BioRAPTR FRD bulk reagent dispenser. The plate was then centrifuged at 200 × *g* for 1 min. After 60 min at room temperature 2 µL of assay buffer containing 20 µg/mL anti-6xHis acceptor beads and 20 µg/mL streptavidin donor beads was dispensed into every well using a Beckman BioRAPTR FRD bulk reagent dispenser. The plates were then centrifuged at 200 × *g* for 1 min. After an overnight incubation at room temperature the plates were read on a Perkin Elmer Envision multimode plate reader in AlphaScreen mode.

Cell viability assay. A-431 cells were grown in media (DMEM + 10% FBS + 1 × Penicillin/Streptomycin + 2 mM L-glutamine) at 37 °C in a humidified incubator with 5% CO_2 to 70% confluency. They were then washed with DPBS and trypsinized. For the assay the cells were resuspended in media (DMEM + 10% FBS + 1 × Penicillin/Streptomycin + 2 mM L-glutamine) at 125,000 cells/mL. Using a Thermo multidrop combi bulk reagent dispenser 4 µL of cell suspension (500 cells) were dispensed into every well of a 1536 well plate. The plates were centrifuged at 200 × g for 1 min, relidded and incubated overnight at 37 °C with 5% CO_2. The next day using a Labcyte Echo 555 acoustic dispenser 5 nL of MG-132, final in well concentration of 25 µM, were added to columns 1–2, 5 nL of DMSO were added to columns 3–4 and 45–48 and 5 nL of 2 mM compounds in DMSO were added to columns 5–44. The plates were then centrifuged at 200 × g for 1 min, relidded and returned to the incubator. After 48 h 4 µL of room temperature ATP-Lite were added with a Beckman BioRAPTR FRD

bulk reagent dispenser. The plates were centrifuged at 200 × *g* for 1 min and then incubated at room temperature. After 10 min the plates were read using a Perkin Elmer Viewlux multimode plate reader in luminescence mode.

Protein-DNA interaction ELISA (PDI-ELISA) assay. The PDI-ELSA assays were described previously[33] and used to determine the inhibition IC_{50} against HMGA2-DNA interactions. The apparent inhibitory IC_{50} values were obtained using the following equation: $y = min + (\frac{(max-min)}{1+10^{((x-logIC_{50})\times Hillslope}})$, where x, y, max, and min represent the inhibitor's concentration, the inhibition level, the maximum inhibition value, and the minimum inhibition value, respectively.

Isothermal titration calorimetry (ITC). ITC experiments were conducted using a VP-ITC titration calorimeter (MicroCal, Inc., Northampton, MA) interfaced to a PC. Origin 7.0, supplied by the manufacturer was used for data acquisition. For a typical ITC experiment, the titration was set up so that 10 µL of 0.2 mM suramin or analogs was injected every 120 s, up to a total of 29 injections, into an HMGA2 sample (1.44 mL of 5 µM) or ATHP3 sample (1.44 mL of 15 µM) in the sample cell in 10 mM Tris–HCl pH 8.0 and 1 mM EDTA. The heat liberated or absorbed is observed as a peak corresponding to the power required keeping the sample and reference cells at identical temperatures. The peak produced during the injection is converted to heat output by integration and corrected for cell volume and sample concentration. Control experiments were also carried out to determine the contribution of the heats of dilution arising from (1) suramin or analogs into buffer and (2) buffer into HMGA2 or ATHP3. The net enthalpy for the titration reaction was determined by subtraction of the component heats of dilution.

Native mass spectrometry. A custom-built nano electrospray unit (nESI) was coupled to a Maxis Impact HD Q-TOF mass spectrometer (Bruker, Billerica, MA) for all the native mass spectrometry analysis. Quartz glass capillaries (O.D.: 1.0 mm and I.D.: 0.70 mm) were pulled utilizing a P-2000 micropipette laser puller (Sutter Instruments, Novato, CA) and loaded with 10 µL aliquot of the sample solution. Sample solutions consisted of 1–10 µM HMGA2 in 10 mM ammonium acetate solution at physiological pH (pH = 6.7). For the observation of the HMGA2-Ligand complexes, a 1:1, 1:3 and 1:10 ratio of 5 µM concentration of the HMGA2 and Ligand (suramin) were prepared in 10 mM ammonium acetate and let it rest for 10 min prior infusion. A typical nESI source voltage of +/− 600–1200 V was applied between the pulled capillary tips and the MS instrument inlet. Ions were introduced via a stainless-steel tube (1/16 × 0.020″, IDEX Health Science, Oak Harbor, WA) held at room temperature into the TIMS cell. Solvents, methanol, and ammonium acetate salts utilized in this study were analytical grade or better and purchased from Fisher Scientific (Pittsburgh, PA). A Tuning Mix calibration standard (G24221A) was obtained from Agilent Technologies (Santa Clara, CA) and used as received. Mass spectra were processed using Bruker Compass Data Analysis version 5.1 (Bruker Daltonik GmbH).

Cell cultures and growth curves. BTSC#83 and BTSC#30p and their culture conditions have been described[38]. For growth curves, suspension cultures were mechanically disaggregated and filtered through 37 µm filters (StemCell Technologies, Vancouver, Canada) in order to obtain *bona fide* single-cell suspension. 1×10^3 cells were plated in U-bottom 96-well plates and treated or not with 100, 200 and 400 µM Suramin. Cell growth was assayed at the indicated time using the CellTiter Assay System (Promega). The growth conditions of 8505c anaplastic thyroid carcinoma cells and mouse Embryonic Fibroblasts (MEFs) knock-out for HMGA1, HMGA2, and HMGA1/A2 double mutant have been described previously[42,64]. P values were calculated by using two-way ANOVA followed by Sidak's multiple comparison test.

Protein extraction and Western blot. The single-cell suspension was obtained by mechanical disaggregation of the spheres and total proteins were extracted 48 h later, as previously described[38]. After separation by SDS–polyacrylamide gel electrophoresis, proteins were blotted on nitrocellulose membranes (GE Healthcare Europe Gmb) and hybridized with the following antibodies: anti-HMGA1, anti-HMGA2 (Genetex) or affinity-purified anti-HMGA2, anti-α-actin (SantaCruz Biotechnologies).

RNA extraction and qRT-PCR analyses. The single-cell suspension was obtained by mechanical disaggregation of the spheres and RNA was extracted 48 h later, by using Direct-zol RNA MiniPrep (Zymo Research). One µg of RNA was retrotranscribed, by using QuantiTect® Reverse Transcription Kit (Qiagen) and qRT-PCR was performed as described[38]. Primers used in the qRT-PCR experiments are listed in Table S3. The $2^{-\Delta\Delta Ct}$ formula was used to calculate the differential gene expression.

Chromatin immunoprecipitation (ChIP) assay. Chromatin immunoprecipitation was performed as described[65]. Briefly, for each sample, 5×10^6 cells were collected by trypsinization and cross-linked with 1% formaldehyde; after sonication, the samples were immunoprecipitated with 10 µL anti-HMGA2 antibody (Genetex) or with control normal rabbit IgG and the chromatin was extracted. qPCR amplification was performed on 6 µL of immunoprecipitated DNA, using primers amplifying regions A and B of the ID2 promoter (Table S2). C_t values of samples precipitated with anti-HMGA2 and IgG antibodies were normalized with C_t values of input DNA. Fold change enrichment was calculated in comparison to normalized IgG, using the $2^{-\Delta\Delta Ct}$ formula. P values were calculated by using one-way ANOVA followed by Sidak's multiple comparison test.

Molecular dynamics simulation. Since HMGA2 is shown to be an intrinsically disordered protein, we first performed molecular dynamics (MD) simulations to generate multiple disordered conformations of

the suramin-interacting segment of HMGA2 chain (–GEKRPRGRPRKW–). Using the Charmm-Gui web interface[66], the peptide was solvated in a cubic water box with TIP3 water and the system was neutralized by adding five Cl^- ions. The final system contained ~ 16,000 atoms. NAMD 2.12[67] was used to perform all-atom molecular dynamics with CHARMM36 force field[68]. The particle mesh Ewald (PME) method[69] was used for calculating the long-range ionic interactions. The system was minimized for 10,000 steps, followed by a 100 ps equilibration at 300 K with 1 fs time step. A 100-ns production simulation with 2-fs time step was performed at a constant pressure of 1 atm. and T = 300 K. The Nose–Hoover Langevin-piston method[70] was used for pressure coupling, with a piston period of 50 fs and a decay of 25 fs, and the Langevin temperature coupling with a friction coefficient of 1 ps^{-1} was used for maintaining the temperature. From the 100-ns simulation trajectory, 1000 protein pdb frames were extracted using Visual Molecular Dynamics (VMD)[71].

In silico docking studies. Suramin was docked to 1000 MD-generated conformations using AutoDock Vina 1.1.2[72]. The protein pdb files and the suramin compound structure were first converted to pdbqt format for docking. Using custom scripts, Suramin was screened against the protein conformations and the resulting scores of the complexes were sorted and ranked according to their binding affinities.

Received: 15 August 2020; Accepted: 19 October 2020
Published online: 02 November 2020

References

1. Zhou, X., Benson, K. F., Ashar, H. R. & Chada, K. Mutation responsible for the mouse pygmy phenotype in the developmentally regulated factor HMGI-C. *Nature* **376**, 771–774 (1995).
2. Anand, A. & Chada, K. In vivo modulation of Hmgic reduces obesity. *Nat. Genet.* **24**, 377–380 (2000).
3. Chung, J. *et al.* High mobility group A2 (HMGA2) deficiency in pigs leads to dwarfism, abnormal fetal resource allocation, and cryptorchidism. *Proc. Natl. Acad. Sci. USA* **115**, 5420–5425 (2018).
4. Sun, T., Fu, M., Bookout, A. L., Kliewer, S. A. & Mangelsdorf, D. J. MicroRNA let-7 regulates 3T3-L1 adipogenesis. *Mol. Endocrinol.* **23**, 925–931 (2009).
5. Fedele, M. *et al.* Role of the high mobility group A proteins in human lipomas. *Carcinogenesis* **22**, 1583–1591 (2001).
6. Ligon, A. H. & Morton, C. C. Genetics of uterine leiomyomata. *Genes Chromosomes Cancer* **28**, 235–245 (2000).
7. Rogalla, P., Drechsler, K., Schroder-Babo, W., Eberhardt, K. & Bullerdiek, J. HMGIC expression patterns in non-small lung cancer and surrounding tissue. *Anticancer Res.* **18**, 3327–3330 (1998).
8. Kumar, M. S. *et al.* HMGA2 functions as a competing endogenous RNA to promote lung cancer progression. *Nature* **505**, 212–217 (2014).
9. Marquis, M. *et al.* High expression of HMGA2 independently predicts poor clinical outcomes in acute myeloid leukemia. *Blood Cancer J.* **8**, 68 (2018).
10. Murakami, M., Suzuki, M., Nishino, Y. & Funaba, M. Regulatory expression of genes related to metastasis by TGF-beta and activin A in B16 murine melanoma cells. *Mol. Biol. Rep.* **37**, 1279–1286 (2010).
11. Raskin, L. *et al.* Transcriptome profiling identifies HMGA2 as a biomarker of melanoma progression and prognosis. *J. Invest Dermatol.* **133**, 2585–2592 (2013).
12. Abe, N. *et al.* Determination of high mobility group I(Y) expression level in colorectal neoplasias: A potential diagnostic marker. *Cancer Res.* **59**, 1169–1174 (1999).
13. Meyer, B. *et al.* HMGA2 overexpression in non-small cell lung cancer. *Mol. Carcinog.* **46**, 503–511 (2007).
14. Fusco, A. & Fedele, M. Roles of HMGA proteins in cancer. *Nat. Rev. Cancer* **7**, 899–910 (2007).
15. Miao, Y., Cui, T., Leng, F. & Wilson, W. D. Inhibition of high-mobility-group A2 protein binding to DNA by netropsin: A biosensor-surface plasmon resonance assay. *Anal. Biochem.* **374**, 7–15 (2008).
16. Nishino, J., Kim, I., Chada, K. & Morrison, S. J. Hmga2 promotes neural stem cell self-renewal in young but not old mice by reducing p16Ink4a and p19Arf expression. *Cell* **135**, 227–239 (2008).
17. Copley, M. R. *et al.* The Lin28b-let-7-Hmga2 axis determines the higher self-renewal potential of fetal haematopoietic stem cells. *Nat. Cell Biol.* **15**, 916–925 (2013).
18. Weedon, M. N. *et al.* A common variant of HMGA2 is associated with adult and childhood height in the general population. *Nat. Genet.* **39**, 1245–1250 (2007).
19. Stein, J. L. *et al.* Identification of common variants associated with human hippocampal and intracranial volumes. *Nat. Genet.* **44**, 552–561 (2012).
20. Reeves, R. Nuclear functions of the HMG proteins. *Biochim. Biophys. Acta* **1799**, 3–14 (2010).
21. Cleynen, I. & Van de Ven, W. J. The HMGA proteins: A myriad of functions (review). *Int. J. Oncol.* **32**, 289–305 (2008).
22. Bianchi, M. E. & Beltrame, M. Upwardly mobile proteins. Workshop: The role of HMG proteins in chromatin structure, gene expression and neoplasia. *EMBO Rep.* **1**, 109–114 (2000).
23. Friedmann, M., Holth, L. T., Zoghbi, H. Y. & Reeves, R. Organization, inducible-expression and chromosome localization of the human HMG-I(Y) nonhistone protein gene. *Nucleic Acids Res.* **21**, 4259–4267 (1993).
24. Manfioletti, G. *et al.* cDNA cloning of the HMGI-C phosphoprotein, a nuclear protein associated with neoplastic and undifferentiated phenotypes. *Nucleic Acids Res.* **19**, 6793–6797 (1991).
25. Zhou, X. *et al.* Genomic structure and expression of the murine Hmgi-c gene. *Nucleic Acids Res.* **24**, 4071–4077 (1996).
26. Cui, T. & Leng, F. Specific recognition of AT-rich DNA sequences by the mammalian high mobility group protein AT-hook 2: A SELEX study. *Biochemistry* **46**, 13059–13066 (2007).
27. Lehn, D. A., Elton, T. S., Johnson, K. R. & Reeves, R. A conformational study of the sequence specific binding of HMG-I (Y) with the bovine interleukin-2 cDNA. *Biochem. Int.* **16**, 963–971 (1988).
28. Reeves, R. & Nissen, M. S. The A.T-DNA-binding domain of mammalian high mobility group I chromosomal proteins. A novel peptide motif for recognizing DNA structure. *J. Biol. Chem.* **265**, 8573–8582 (1990).
29. Frost, L. *et al.* The dimerization state of the mammalian high mobility group protein AT-hook 2 (HMGA2). *PLoS ONE* **10**, e0130478 (2015).
30. Huth, J. R. *et al.* The solution structure of an HMG-I(Y)-DNA complex defines a new architectural minor groove binding motif. *Nat. Struct. Biol.* **4**, 657–665 (1997).
31. Reeves, R. & Beckerbauer, L. M. HMGA proteins as therapeutic drug targets. *Prog. Cell Cycle Res.* **5**, 279–286 (2003).

32. Chen, B., Young, J. & Leng, F. DNA bending by the mammalian high-mobility group protein AT hook 2. *Biochemistry* **49**, 1590–1595 (2010).
33. Alonso, N., Guillen, R., Chambers, J. W. & Leng, F. A rapid and sensitive high-throughput screening method to identify compounds targeting protein-nucleic acids interactions. *Nucleic Acids Res.* **43**, e52 (2015).
34. Barrett, M. P. & Gilbert, I. H. Targeting of toxic compounds to the trypanosome's interior. *Adv. Parasitol.* **63**, 125–183 (2006).
35. Cui, T. *et al.* Large scale preparation of the mammalian high mobility group protein A2 for biophysical studies. *Protein Pept. Lett.* **14**, 87–91 (2007).
36. Thuault, S. *et al.* Transforming growth factor-beta employs HMGA2 to elicit epithelial–mesenchymal transition. *J. Cell Biol.* **174**, 175–183 (2006).
37. Thuault, S. *et al.* HMGA2 and Smads co-regulate SNAIL1 expression during induction of epithelial-to-mesenchymal transition. *J. Biol. Chem.* **283**, 33437–33446 (2008).
38. Colamaio, M. *et al.* HMGA1 silencing reduces stemness and temozolomide resistance in glioblastoma stem cells. *Expert Opin. Ther. Targets* **20**, 1169–1179 (2016).
39. Puca, F. *et al.* HMGA1 negatively regulates NUMB expression at transcriptional and post transcriptional level in glioblastoma stem cells. *Cell Cycle* **18**, 1446–1457 (2019).
40. Zhang, Y. L., Keng, Y. F., Zhao, Y., Wu, L. & Zhang, Z. Y. Suramin is an active site-directed, reversible, and tight-binding inhibitor of protein-tyrosine phosphatases. *J. Biol. Chem.* **273**, 12281–12287 (1998).
41. McGeary, R. P., Bennett, A. J., Tran, Q. B., Cosgrove, K. L. & Ross, B. P. Suramin: Clinical uses and structure–activity relationships. *Mini. Rev. Med. Chem.* **8**, 1384–1394 (2008).
42. Federico, A. *et al.* Hmga1/Hmga2 double knock-out mice display a "superpygmy" phenotype. *Biol. Open* **3**, 372–378 (2014).
43. Buscher, P., Cecchi, G., Jamonneau, V. & Priotto, G. Human African trypanosomiasis. *Lancet* **390**, 2397–2409 (2017).
44. Wainwright, M. Dyes, trypanosomiasis and DNA: A historical and critical review. *Biotech. Histochem.* **85**, 341–354 (2010).
45. Darnell, J. E. Jr. Transcription factors as targets for cancer therapy. *Nat. Rev. Cancer* **2**, 740–749 (2002).
46. Cagel, M., Grotz, E., Bernabeu, E., Moretton, M. A. & Chiappetta, D. A. Doxorubicin: Nanotechnological overviews from bench to bedside. *Drug Discov. Today* **22**, 270–281 (2017).
47. Riddell, I. A. Cisplatin and oxaliplatin: Our current understanding of their actions. *Met. Ions Life Sci.* **18**, 1–42 (2018).
48. Meredith, A. M. & Dass, C. R. Increasing role of the cancer chemotherapeutic doxorubicin in cellular metabolism. *J. Pharm. Pharmacol.* **68**, 729–741 (2016).
49. Yan, C. & Higgins, P. J. Drugging the undruggable: Transcription therapy for cancer. *Biochim. Biophys. Acta* **1835**, 76–85 (2013).
50. Reeves, R. Molecular biology of HMGA proteins: Hubs of nuclear function. *Gene* **277**, 63–81 (2001).
51. Reeves, R. & Beckerbauer, L. HMGI/Y proteins: Flexible regulators of transcription and chromatin structure. *Biochim. Biophys. Acta* **1519**, 13–29 (2001).
52. Dressel, J. R. E. O. The discovery of Germanin by Oskar Dressel and Richard Kothe. *J. Chem. Educ.* **38**, 620 (1961).
53. Barrett, M. P., Boykin, D. W., Brun, R. & Tidwell, R. R. Human African trypanosomiasis: Pharmacological re-engagement with a neglected disease. *Br. J. Pharmacol.* **152**, 1155–1171 (2007).
54. Fairlamb, A. H. & Bowman, I. B. Uptake of the trypanocidal drug suramin by bloodstream forms of *Trypanosoma brucei* and its effect on respiration and growth rate in vivo. *Mol. Biochem. Parasitol.* **1**, 315–333 (1980).
55. Scott, A. G., Tait, A. & Turner, C. M. Characterisation of cloned lines of *Trypanosoma brucei* expressing stable resistance to MelCy and suramin. *Acta Trop.* **60**, 251–262 (1996).
56. Opperdoes, F. R. Compartmentation of carbohydrate metabolism in trypanosomes. *Annu. Rev. Microbiol.* **41**, 127–151 (1987).
57. Jensen, R. E. & Englund, P. T. Network news: The replication of kinetoplast DNA. *Annu. Rev. Microbiol.* **66**, 473–491 (2012).
58. Wilson, W. D. *et al.* Antiparasitic compounds that target DNA. *Biochimie* **90**, 999–1014 (2008).
59. Wang, J., Pappas-Brown, V., Englund, P. T. & Jensen, R. E. TbKAP6, a mitochondrial HMG box-containing protein in *Trypanosoma brucei*, is the first trypanosomatid kinetoplast-associated protein essential for kinetoplast DNA replication and maintenance. *Eukaryot. Cell* **13**, 919–932 (2014).
60. Kaur, M., Reed, E., Sartor, O., Dahut, W. & Figg, W. D. Suramin's development: What did we learn?. *Invest. New Drugs* **20**, 209–219 (2002).
61. La Rocca, R. V., Stein, C. A., Danesi, R. & Myers, C. E. Suramin, a novel antitumor compound. *J. Steroid Biochem. Mol. Biol.* **37**, 893–898 (1990).
62. Wu, K. *et al.* Suramin inhibits cullin-RING E3 ubiquitin ligases. *Proc. Natl. Acad. Sci. USA* **113**, E2011–E2018 (2016).
63. Wiedemar, N., Hauser, D. A. & Maser, P. 100 years of suramin. *Antimicrob. Agents Chemother.* **64**, e01168-19 (2020).
64. Ito, T. *et al.* In vitro irradiation is able to cause RET oncogene rearrangement. *Cancer Res.* **53**, 2940–2943 (1993).
65. Puca, F. *et al.* HMGA1 silencing restores normal stem cell characteristics in colon cancer stem cells by increasing p53 levels. *Oncotarget* **5**, 3234–3245 (2014).
66. Qi, Y. *et al.* CHARMM-GUI Martini maker for coarse-grained simulations with the Martini force field. *J. Chem. Theory Comput.* **11**, 4486–4494 (2015).
67. Phillips, J. C. *et al.* Scalable molecular dynamics with NAMD. *J. Comput. Chem.* **26**, 1781–1802 (2005).
68. Huang, J. & MacKerell, A. D. Jr. CHARMM36 all-atom additive protein force field: Validation based on comparison to NMR data. *J. Comput. Chem.* **34**, 2135–2145 (2013).
69. Essmann, U. *et al.* A smooth particle mesh Ewald method. *J. Chem. Phys.* **103**, 8577–8593 (1995).
70. Brooks, M. M., Hallstrom, A. & Peckova, M. A simulation study used to design the sequential monitoring plan for a clinical trial. *Stat. Med.* **14**, 2227–2237 (1995).
71. Humphrey, W., Dalke, A. & Schulten, K. VMD: Visual molecular dynamics. *J. Mol. Graph.* **14**, 33–38 (1996).
72. Trott, O. & Olson, A. J. AutoDock Vina: Improving the speed and accuracy of docking with a new scoring function, efficient optimization, and multithreading. *J. Comput. Chem.* **31**, 455–461 (2010).

Acknowledgements

This work was supported by grants 1R15GM109254-01A1 and 1R21AI125973-01A1 from the National Institutes of Health (to F.L.), and by the Florida Translational Research Program, a contract administered by the Florida Department of Health (COHK8), and for which Layton Smith is the Principal Investigator.

Author contributions

F.L., S.B., S.V., and L. Smith designed research; L.S., N.B. S.B., J.F., A.G., F.D., M.R., F.F. and P.C. performed research; F.L., S.B., A.F., L.K., J.C., F.F.-L., P.C., S.V., and L. Smith analyzed data; F.L. wrote the paper.

Competing interests

The authors declare no competing interests.

Additional information

Supplementary information is available for this paper at https://doi.org/10.1038/s41598-020-75890-0.

Correspondence and requests for materials should be addressed to F.L.

Reprints and permissions information is available at www.nature.com/reprints.

Publisher's note Springer Nature remains neutral with regard to jurisdictional claims in published maps and institutional affiliations.